RSC Advances

PAPER

View Article Online
View Journal | View Issue

Check for updates

Cite this: *RSC Adv.*, 2024, **14**, 32358

Pt/C catalysts synthesized in a commercial particle atomic layer deposition system enabling improved durability in fuel cells

Fiona Pescher,[abcd] Julian Stiegeler,[ad] Philipp A. Heizmann,[abd] Carolin Klose,[ab] Severin Vierrath[abcde] and Matthias Breitwieser*[ae]

Received 28th June 2024
Accepted 2nd October 2024

DOI: 10.1039/d4ra04708g

rsc.li/rsc-advances

Particle atomic layer deposition (ALD) is an emerging method for engineering 3D materials, such as powders, for energy applications. In our study, we employ a commercially available and scalable particle ALD system to synthesize Pt/C electrocatalysts for fuel cells. Our method yields Pt/C catalysts characterized by highly dispersed platinum nanoparticles with a narrow particle size distribution of 2.2 ± 0.5 nm for 30 wt% Pt and 2.6 ± 0.6 nm for 40 wt% Pt, as verified through transmission electron microscopy and X-ray diffraction analysis. The performance of the ALD-synthesized catalysts is benchmarked against a state-of-the-art catalyst (TEC10V50E), with both catalysts exhibiting similar beginning-of-test performance (1.6 A cm^{-2} at 0.65 V) under application-relevant operation conditions (80 °C, 50% relative humidity). After 30 000 voltage cycles, conducted in accordance with the U.S. Department of Energy's accelerated catalyst degradation test, the ALD catalysts demonstrate up to 64% greater electrochemical active surface areas and superior retention of cell performance, with a 34% higher current density at 0.65 V, compared to the reference. Given the scalability of the commercial particle ALD system, these promising results encourage the use of particle ALD as a novel synthesis approach for fuel cell catalyst materials in the industry.

Introduction

Despite their small number, heavy-duty vehicles contribute approximately 25% of the total CO_2 emissions from the transportation sector in Europe. Therefore, the electrification of this sector *via* battery- or fuel cell-powered vehicles is key to meet the decarbonization goals.[1] The development of high-performing and stable catalysts remains one of the major challenges for durable proton-exchange membrane (PEM) fuel cells in heavy-duty applications.[2,3] High stability and mass activities can be achieved with platinum nanoparticles supported on porous carbon supports (Pt/C).[4–6] However, these systems still suffer from various degradation processes during operation, such as Ostwald ripening of the catalyst particles and carbon corrosion.[5–8]

Different approaches to enhance the stability of Pt based catalysts have been extensively studied in literature.[8–14] Recently, the synthesis of catalyst powders with the aid of atomic layer deposition (ALD) has been introduced as a promising alternative to conventional wet chemical methods to counteract these degradation issues and enhance the performance and durability of PEM fuel cells.[15–17] ALD is a surface coating method that utilizes self-limiting half-reactions between a solid substrate surface and gaseous precursor molecules. Typically, two half-reactions separated by vacuuming or purging steps represent one ALD cycle, as shown in Fig. 1(b). By executing a defined number of iterative cycles, nanoparticles or thin films can be grown on the substrate surface with layer-by-layer precision.[17,18]

While traditional ALD approaches focus on coating flat surfaces, specialized reactor concepts have been developed to achieve homogeneous coatings on powder materials.[17–19] For example, in fluidized bed ALD reactors, the powder is contained on top of a mesh and an upward gas flow is used to fluidize the substrate particles. This gas flow also contains the gaseous precursor material, ensuring thorough mixing of the sample and high utilization of the precursor molecules.[17–19] Consequently, nanoparticles or coatings can be deposited remarkably homogeneously onto the substrate surface and within its pores.[15,16,18,20] It has been reported that Pt/C catalysts produced by lab-scale commercial or custom-built fluidized bed ALD

---

[a] *Electrochemical Energy Systems, Laboratory for MEMS Applications, IMTEK – Department of Microsystems Engineering, University of Freiburg, Georges-Koehler-Allee 103, 79110 Freiburg, Germany*

[b] *Hahn-Schickard, Georges-Koehler-Allee 103, 79110 Freiburg, Germany*

[c] *Freiburg Materials Research Center (FMF), University of Freiburg, Stefan-Meier-Straße 21, 79104 Freiburg, Germany*

[d] *Freiburg Center for Interactive Materials and Bioinspired Technologies (FIT), University of Freiburg, Georges-Köhler-Allee 105, 79110 Freiburg, Germany*

[e] *ionysis GmbH, Georges-Koehler-Allee 103, 79110 Freiburg, Germany. E-mail: matthias.breitwieser@ionysis.com*

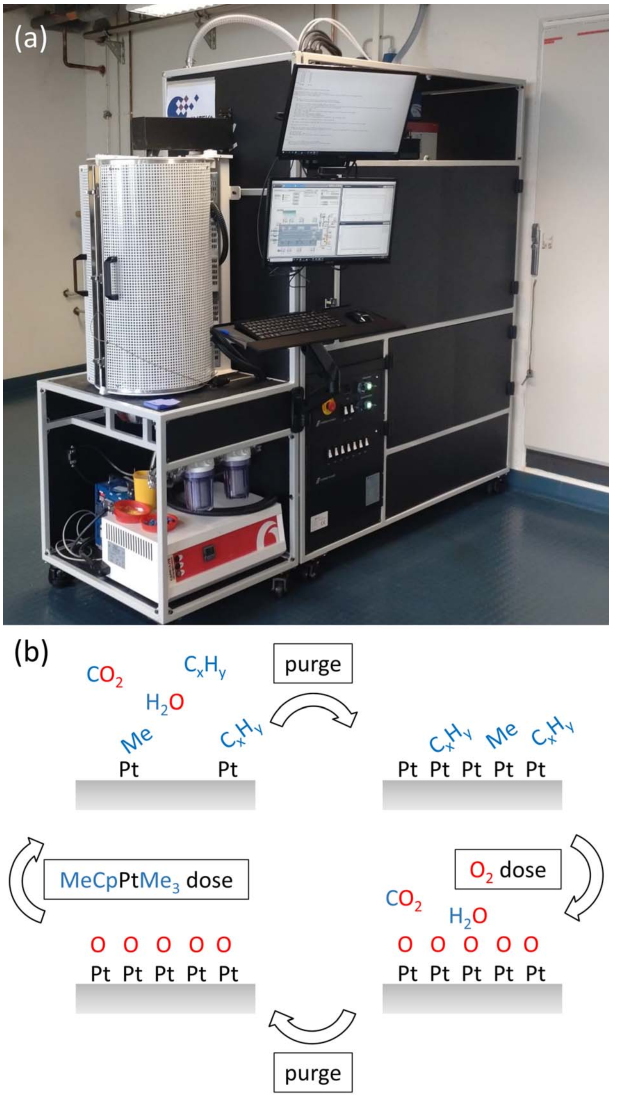

Fig. 1 (a) Prometheus P-8 fluidized bed ALD by Forge Nano. (b) Schematic description of the individual steps within the Pt-ALD process.

reactors can improve the performance of PEM fuel cells compared to conventionally synthesized catalysts[15,20] as well as improve long-term stability over 30 000 cycles.[16]

Today, only a few commercialized particle ALD coating systems are available, allowing for the first time ALD coating of powders in batch sizes ranging from grams to tons.[21,22] In several energy-related applications, such as protective coatings for battery materials, the application of ALD has approached an industrially relevant scale in recent years.[23] Building on these promising results, our study demonstrates the synthesis of platinum nanoparticles on carbon powder using a scalable and commercially available particle ALD system.

Experimental

Electrocatalyst synthesis

Carbon treatment. The carbon black material Vulcan XC72R (Fuel Cell Store) was used as the support material for platinum deposition. To enhance its surface functionalization, the carbon underwent an oxidation process following the methodology outlined by Lee *et al.*[24] Initially, 5 g of citric acid (Thermo Scientific Alfa Aesar, 99+%) was dissolved in 125 mL of deionized water. Subsequently, 5 g of carbon black was added, and the dispersion was stirred for 1 h at room temperature. The resulting mixture was washed *via* centrifugation in a Z 206 A small centrifuge (Hermle Labortechnik GmbH) until the wash solution reached pH neutrality. The sediment was air-dried overnight at 80 °C, followed by heating in an OTF-1200X-S tube furnace (MTI Corporation) for 1 h at 300 °C under a flow of 2 L min^{-1} oxygen and 2 L min^{-1} nitrogen to thermally remove all remaining citric acid residues. The oxidized carbon was then ground and sieved to achieve a particle size of 50–100 μm.

Platinum fluidized bed ALD. Platinum nanoparticles were deposited onto the functionalized carbon black particles using a pilot scale Prometheus P8 fluidized bed ALD system from Forge Nano (Fig. 1(a)).[25,26] The powder is contained within the system *via* a porous distribution plate at the bottom and porous cylindrical filters at the reactor's top. The reactor design, featuring a cylindrical base that widens towards the top, induces a pressure drop, effectively confining the powder bed in the bottom section. A vibrational motor, an impactor, and a jet assist can be used for agitating the powder and helping with its fluidization. The Prometheus ALD is equipped with a residual gas analyzer, the e-Vision 2 (mks Instruments), allowing the observation of reactants and reaction byproducts during the deposition process.

$MeCpPtMe_3$ [trimethyl-(methylcyclopentadienyl)-platinum(IV)] (Strem Chemicals Inc., 99%) was used as the platinum precursor. The chemical was stored in a stainless-steel bubbler, which was heated to 50 °C, and through which a nitrogen flow was passed to help draw vapor from the low vapor pressure material. Ultrapure oxygen gas (Messer Industriegase GmbH, 99.998%) was used as the second reactant. Separate feeding lines were used for O_2 and $MeCpPtMe_3$, with the system lines maintained at temperatures between 130 °C and 145 °C. During the platinum half cycle, the reactor was set to 300 °C, while during the O_2 half cycle, it was kept either at 150 °C, 200 °C, or 300 °C. For each ALD experiment, 200 mg of the pre-processed powder was loaded into the fluidized bed reactor. The powder was contained by two filters with 2 μm pore size, located at the bottom and top of the reactor. Ultrapure N_2 gas (Messer Industriegase GmbH, 99.999%) flowed upwards through the reactor in order to fluidize the powder bed. One ALD cycle consisted of at least 20 min of $MeCpPtMe_3$ dose, during which a constant nitrogen flow of 10 sccm was passed through the bubbler. Afterwards, the reactor was purged for at least 40 min with a 10 sccm N_2 flow. The system was adjusted to the temperature of the oxygen dose (150 °C, 200 °C, or 300 °C), and O_2 was dosed through the reactor for at least 20 min followed by at least 40 min of purging with 14.5 sccm N_2. By monitoring O_2 and CO_2 signals with the residual gas analyzer, conclusions can be drawn regarding the prevalence of carbon combustion during oxygen doses. Carbon combustion could be excluded for the chosen oxygen dose temperature of 150 °C. A vibrational motor was used to shake the reactor during the whole process to ensure a good mixing of the sample. After two to eight cycles of platinum deposition, the system was cooled down, and the Pt/C powder was retrieved from the reactor.

Characterization

Platinum content quantification. The platinum content in each powder sample was determined gravimetrically by heating the samples in an OTF-1200X-S tube furnace (MTI Corporation) under a continuous oxygen flow until all carbon was fully oxidized and removed. Additionally, thermogravimetric analysis (TGA) was conducted under air atmosphere in a range of 30–1000 °C at a heating rate of 10 °C min^{-1} using a STA449 F5 (Netzsch Gerätebau GmbH) for platinum content verification.

Powder X-ray diffraction (XRD). Powder X-ray diffractograms were acquired using a SmartLab diffractometer (Rigaku Corporation) equipped with a copper X-ray source (Kα, λ = 1.541874 Å). The powder samples were prepared on a glass holder and rotated at 120 rpm during measurement. A 2θ range from 15° to 120° was measured with a step size of 0.01° and a speed of 5° per minute using a HyPix-3000HE Hybrid Pixel 2D array detector (Rigaku Corporation). The average crystallite size was calculated from the diffractogram using the (220) reflex at 67° and the Scherrer equation[27–29] with a shape factor of K = 0.94.

Transmission electron microscopy (TEM). Samples were dispersed in isopropyl alcohol, briefly sonicated using a Sonorex Super RK 100 H ultrasonic bath (Bandelin electronic GmbH & Co. KG), and loaded onto copper TEM grids (lacey carbon film, 200 mesh, Science Services GmbH) by dip coating. The TEM grids were dried in air.

TEM micrographs were captured using a Talos L120C TEM (Thermo Fisher Scientific) equipped with a LaB6 electron source and operated at a 120 kV accelerating voltage, and a Talos F200X (S)TEM (Thermo Fisher Scientific) with a high-brightness X-FEG emitter, operated at an acceleration voltage of 200 kV. Both instruments utilized Ceta 16 Megapixel CMOS Cameras at approximately 1 nA current. Dark-field (S)TEM micrographs were captured using a high-angle annular dark-field detector. *D*-spacing values were calculated from the fast furrier transform diffraction patterns of high-resolution (HR)-TEM micrographs.

For the determining the platinum nanoparticle size distribution, 500 nanoparticles were measured to ensure quantitative accuracy. Nanoparticle size distributions for each sample were analyzed using ImageJ 1.54 h.

Electrochemical fuel cell testing

Fabrication of membrane electrode assemblies. Commercial Pt/C catalysts used as reference catalysts for electrochemical fuel cell tests were procured from Umicore AG & Co. KG and Tanaka Kikinzoku Kogyo K.K. The 3 M PFSA ionomer was supplied by 3 M, and PFSA FS715RFS membranes were supplied by Fumatech BWT GmbH.

For the fabrication of membrane electrode assemblies (MEA), anode catalyst inks (2 wt% solids in a 1 : 4 w/w IPA/water mixture) were prepared using commercial Pt/C (47 wt% Pt content, Elyst Pt50 0550, Umicore AG & Co. KG) and an ionomer-to-carbon ratio (I/C) of 0.5. A similar ink containing TEC10V50E Pt/C (47 wt% Pt content, Tanaka Kikinzoku Kogyo K.K.) was used for reference cathodes. The most promising catalysts synthesized *via* fluidized bed ALD were also processed into inks with the same I/C ratio of 0.5.

The catalyst layers were applied onto pristine commercial Fumapem® FS715RFS membranes (725 EW, mechanically reinforced, chemically stabilized, 15 μm nominal thickness) using an automated ultrasonic spray-coating system (Nebular, BioFluidix GmbH). The fabricated MEAs had an area of 4 cm^2. The platinum loading of all MEAs was 0.1 mg cm^{-2} for the anode and 0.4 mg cm^{-2} for the cathode side. The loadings were verified *via* micro X-ray fluorescence using an M4 Tornado (Bruker Corporation).

Characterization of membrane electrode assemblies. For fuel cell assembly, the MEA was placed between two gas diffusion layers (H14Cx653, Freudenberg Performance Materials GmbH & Co. KG). Glass-fiber reinforced PTFE spacers (Böhme Kunststofftechnik GmbH & Co. KG, 125 μm nominal thickness) were used to establish compression. The MEAs were then built into fuel cell test fixtures (Scribner, LLC), featuring a custom-built 4 cm^2 parallel graphite flow field setup in a cross-flow configuration. Clamping force was regulated by applying 10 Nm torque across the eight M6 rods of the fixture. The fixture was attached to a fuel cell test station (850e, Scribner, LLC).

The cells underwent a break-in procedure (80 °C, H_2/O_2, 0.25/0.50 slpm, 100% relative humidity (RH), ambient pressure, open cell voltage −0.2–0.5 V, 30 s hold time at each potential, 60 cycles)[30,31] and voltage recovery (55 °C, H_2/air, 0.25/1.00 slpm, 200% RH, ambient pressure, 0.08–0.12 V, 20 s hold time at each potential, 180 cycles).[32,33]

Accelerated stress tests (AST), based on the protocol proposed by the U.S. Department of Energy (DOE) for Pt dissolution, were conducted to test the electrocatalyst stability, focusing on platinum degradation.[34] The voltage was cycled between 0.6 V and 0.95 V, using 0.5 s ramp times and 2.5 s hold times for each potential (80 °C, H_2/N_2, 0.05/0.02 slpm, 100% RH, ambient pressure).

At the beginning of test, after 100, 1000, 10 000 and 30 000 cycles, cyclic voltammograms (CV) (80 °C, H_2/N_2, 0.20/0.00 slpm, 100% RH, ambient pressure, 0.06–0.80 V, 50 mV s^{-1}, 8 cycles) were measured. The median of the CV cycles 2 to 7 was considered for the determination of the electrochemically active surface area (ECSA). The ECSA was calculated from the integrated hydrogen adsorption peak assuming a charge of 210 μC cm^{-2}.[33,35–37]

H_2/O_2 polarization curves (80 °C, 0.25/1.00 slpm, 100% RH, 50 kPa back pressure, 0–100 mA cm^{-2}, 5 mA cm^{-2} steps) were recorded at the beginning of test, after 100, 1000, 10 000 and 30 000 cycles. Mass activities were obtained at 0.9 V and corrected for high-frequency resistances (membrane, contact, and electronic resistances) and for hydrogen crossover.[32,37,38] Specific activities were calculated from mass activity and ECSA values. The Tafel slopes were obtained from the polarization curves and corrected for high-frequency resistances and for hydrogen crossover.[32,37,39]

The hydrogen crossover was determined by linear sweep voltammetry (80 °C, H_2/N_2, 0.20/0.05 slpm, 100% RH, 50 kPa back pressure, 0.0–0.6 V, 1 mV s^{-1}).[32,33,37]

H_2/air polarization measurements (80 °C, 0.25/1.00 slpm, 50% RH, 130 kPa back pressure) were performed at the beginning of the test (BOT) and the end of the test (EOT).[30]

Results and discussion

Process temperature optimization

The platinum deposition process employed $MeCpPtMe_3$ and O_2 as precursors, as illustrated in Fig. 1(b). While existing literature suggests a reactor temperature of 300 °C for this system,[15,16,40,41] operational temperatures may vary depending on the individual reactor design utilized. Challenges such as carbon combustion and mass loss have been documented for oxygen-based Pt-ALD onto Vulcan XC72R[41] and for the thermal and ozone-based deposition of platinum onto Ketjenblack EC-300J.[42] To address these challenges in our commercial ALD system, the temperature of the oxygen dose was varied (300 °C, 200 °C, 150 °C) while maintaining the platinum precursor dose at 300 °C. This approach ensures sufficient platinum deposition rates while preventing the condensation of organic precursor molecules within the reactor system.[40]

The yield of each ALD process is detailed in Table 1. While the samples subjected to oxygen doses at 200 °C and 300 °C experienced a decrease in mass due to carbon combustion, counteracting the mass intake from platinum deposition, the 150 °C sample exhibited the expected mass increase. The platinum content in each sample was determined gravimetrically and is provided in Table 1. The higher platinum content observed with increasing oxygen dose temperature does not stem from enhanced platinum deposition rates but rather from parts of the carbon support combusting during the oxygen dose, leading to a higher ratio of platinum remaining in the sample.

Bright-field and dark-field TEM micrographs of the ALD samples are presented in Fig. 2 and 3. The sample prepared completely at a reactor temperature of 300 °C exhibits uniformly dispersed nanoparticles across the entire carbon surface, alongside significantly larger agglomerates (highlighted by yellow arrows). Partial combustion of the carbon support during the oxygen dose causes the already deposited platinum nanoparticles to agglomerate into larger particles, consistent with literature findings.[41] In the ALD-Pt/C-200 °C sample (Fig. 2/3(b)), again, evenly distributed nanoparticles can be observed alongside bigger platinum agglomerates. These agglomerates are comparatively smaller than those in the 300 °C sample, indicating a reduction, but not a complete suppression, in substrate combustion at lower temperatures. Notably, the ALD-Pt/C-150 °C catalyst (Fig. 2/3(c)) exhibits solely supported nanoparticles (2.2 ± 0.5 nm, TEM) without any platinum agglomerates. HR-TEM micrographs of non-agglomerated platinum particles are depicted in Fig. 4. All Pt/Cs show a lattice spacing of 0.22 nm, which corresponds to the (111) facet of platinum.[15,43,44]

Table 1 Yield of the ALD processes and TGA platinum content of the prepared ALD-Pt–C samples, as well as crystallite size of the platinum particles determined from XRD patterns

Sample	Yield [%]	Pt content [wt%]	Crystallite size [nm]
ALD-Pt/C-300 °C	36	78	21.7
ALD-Pt/C-200 °C	95	32	6.7
ALD-Pt/C-150 °C	139	28	2.1

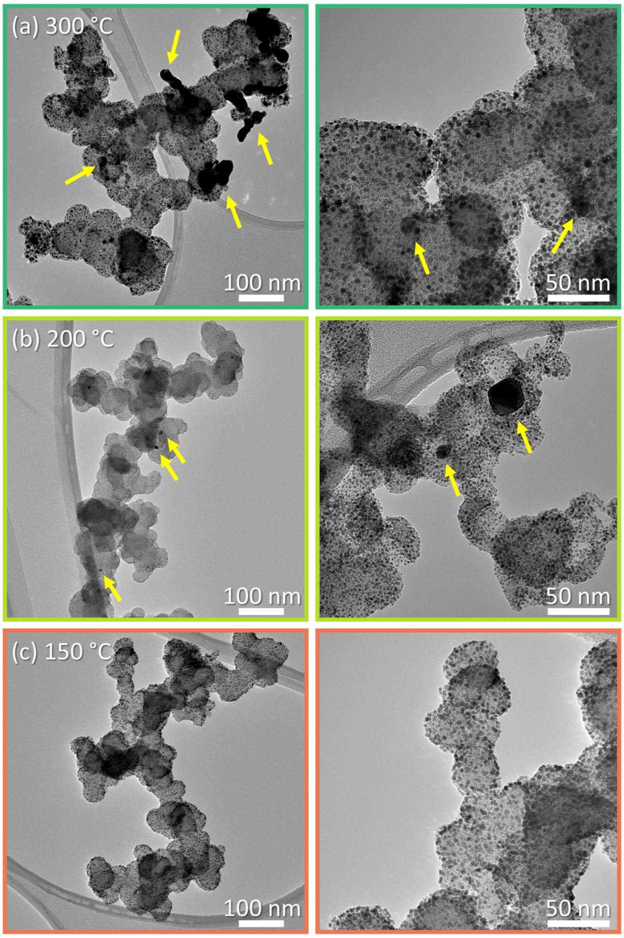

Fig. 2 Bright-field TEM micrographs of ALD Pt/Cs, synthesized with different oxygen dose temperatures: (a) ALD-Pt/C-300 °C, (b) ALD-Pt/C-200 °C, and (c) ALD-Pt/C-150 °C. Yellow arrows indicate the presence of platinum agglomerations. The process temperature of (c) 150 °C was chosen for all further ALD and fuel cell experiments.

Powder X-ray diffractograms of the catalysts are provided in Fig. 5. The sample coated at an oxygen dosing temperature of 300 °C exhibits well-defined diffraction peaks, indicating the presence of significant platinum bulk particles. The diffraction peaks at $2\theta = 39.7°$, 46.2°, 67.4°, 81.2°, and 85.7° correspond to the indexed planes (111), (200), (220), (311), and (222), respectively, consistent with the face-centered cubic (fcc) structure of platinum.[45–48] These bulk particles are also observed with TEM, as previously shown in Fig. 2(a). In contrast, the sample subjected to the lowest oxygen dose temperature of 150 °C exhibits broadened diffraction signals, characteristic of crystallites with a low finite size as expected with the formation of nanoparticles.[27] This is consistent with the observations from TEM micrographs, where solely nanoparticles are visible in this sample (Fig. 2(c)). The ALD-Pt/C-200 °C sample shows a bimodal size distribution, with sharp reflexes superimposed with broad reflections, indicating the presence of both platinum

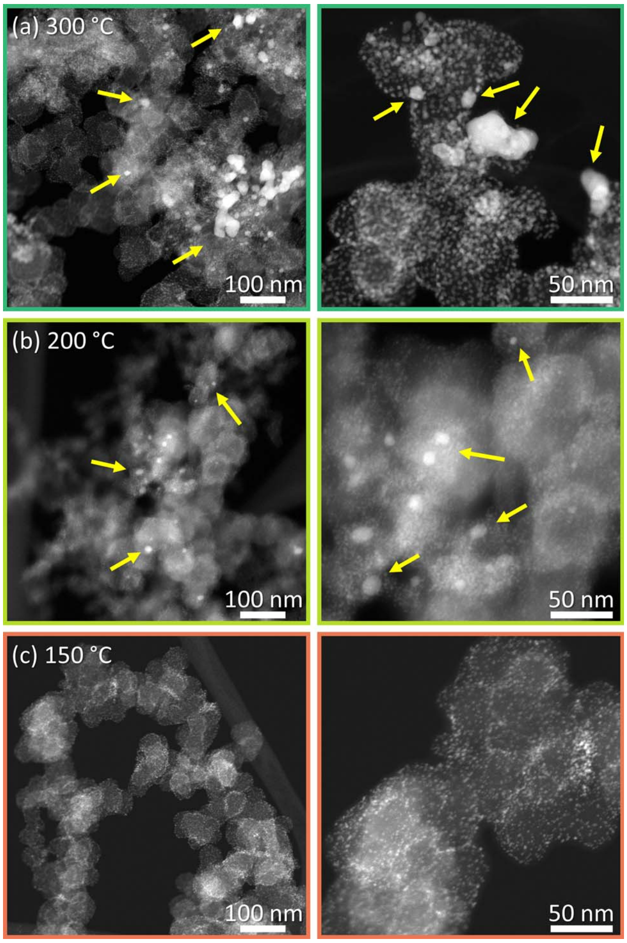

Fig. 3 Dark-field TEM micrographs of ALD Pt/Cs, synthesized with different oxygen dose temperatures: (a) ALD-Pt/C-300 °C, (b) ALD-Pt/C-200 °C, and (c) ALD-Pt/C-150 °C. Yellow arrows indicate the presence of platinum agglomerations.

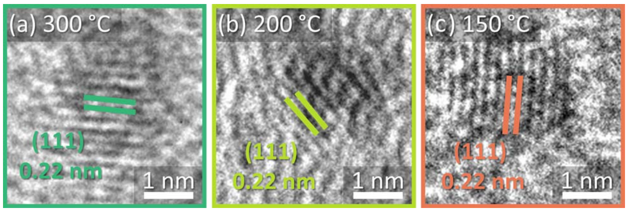

Fig. 4 HR-TEM micrographs of non-agglomerated Pt nanoparticles of ALD Pt/Cs, synthesized with different oxygen dose temperatures: (a) ALD-Pt/C-300 °C, (b) ALD-Pt/C-200 °C, and (c) ALD-Pt/C-150 °C.

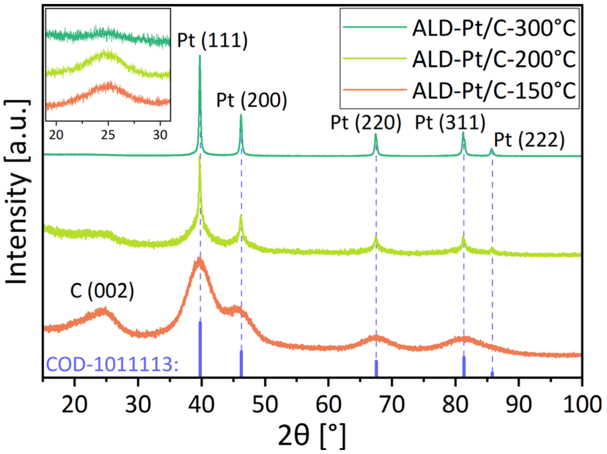

Fig. 5 Powder XRD pattern of the Pt/Cs prepared *via* ALD.

nanoparticles and bulk platinum. This is as expected, as higher deposition temperatures promote carbon oxidation, leading to the formation of platinum bulk particles. Conversely, reducing the temperature prevents carbon corrosion, thereby inhibiting the agglomeration of platinum nanoparticles. The diffraction peak at $2\theta = 24^\circ$ corresponds to the index plane (002) of the carbon support.[16,48,49] With increasing degree of carbon support combustion, the intensity of the signal decreases. The platinum crystallite sizes of the samples were determined from the reflex at $2\theta = 67^\circ$ (220) using the Scherrer equation[27] and are provided in Table 1. For the samples associated with carbon combustion, these values should be viewed with caution, as these samples exhibit a bimodal distribution of platinum particles (comprising both nanoparticles as well as bulk particles). The ALD-Pt/C-150 °C catalyst shows nanoparticles with an average crystallite size of 2.1 nm, in accordance with the particle size seen in the TEM micrographs (2.2 ± 0.5 nm). Thus, by reducing the oxygen dose temperature to 150 °C, the combustion of the carbon support has been successfully inhibited and Pt/Cs with highly dispersed platinum nanoparticles exhibiting a narrow size distribution were successfully synthesized. Therefore, an oxygen dose temperature of 150 °C was chosen for all further ALD experiments.

Influence of cycle numbers on platinum deposition

The cycle number of the platinum deposition process implementing a low temperature oxygen dose was varied between two to eight cycles to achieve different loadings of platinum, ranging from 15 wt% to 40 wt%, on the carbon support. The platinum contents were verified through TGA and are given in

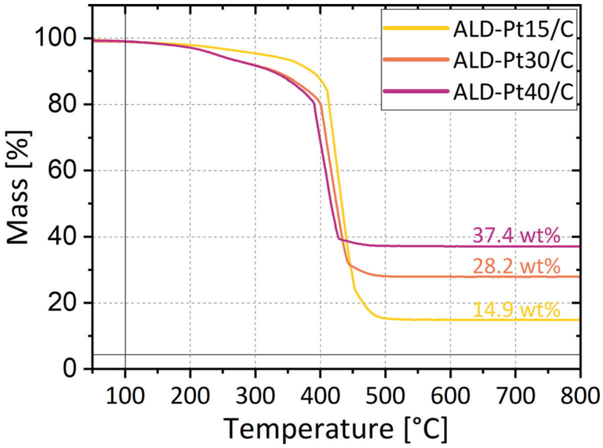

Fig. 6 TGA curves of the Pt/C catalysts prepared with different numbers of ALD cycles.

Table 2 Platinum content of the prepared ALD-Pt/C samples obtained from TGA, as well as the size of the platinum particles determined from TEM micrographs and XRD patterns

Sample	Number of ALD cycles	Pt content (from TGA) [wt%]	Particle size (from TEM) [nm]	Crystallite size (from XRD) [nm]
ALD-Pt15/C	2	14.9	1.9 ± 0.4	1.8
ALD-Pt30/C	5	28.2	2.2 ± 0.5	2.1
ALD-Pt40/C	8	37.4	2.9 ± 0.6	2.6

Fig. 6 and Table 2. With increasing number of ALD cycles, the weight percentage of platinum on carbon increases.

Bright-field TEM micrographs of these catalyst powders are shown in Fig. 7, the corresponding particle size distributions are presented in Fig. 8, and the average particle sizes are provided in Table 2. The tolerance stems from the standard deviation of the histograms. Dark-field TEM micrographs are given in Fig. 9.

The platinum nanoparticles grow in size with an increasing number of ALD cycle, from 1.9 ± 0.4 nm for 15 wt% platinum on carbon up to 2.9 ± 0.6 nm for 40 wt% platinum on carbon, while maintaining a narrow size distribution. With an increased cycle count, a shift of the entire histogram towards larger particle sizes is observed, indicating that the platinum uptake stems from the growth of already deposited nanoparticles rather than the formation of new platinum nucleation sites. This observation is consistent with theoretical expectations, where during the first ALD cycle the platinum precursor reacts with the surface functional groups of the carbon support, forming platinum nucleation sited. In the subsequent cycles, the platinum precursor reacts with oxygen groups attached to the pre-existing platinum nanoparticles, thus increasing their size.[17] For ALD-Pt40/C, the increase in the number of nanoparticles larger than 4 nm is noteworthy. This could be due to platinum particles in close proximity agglomerating and coalescing with

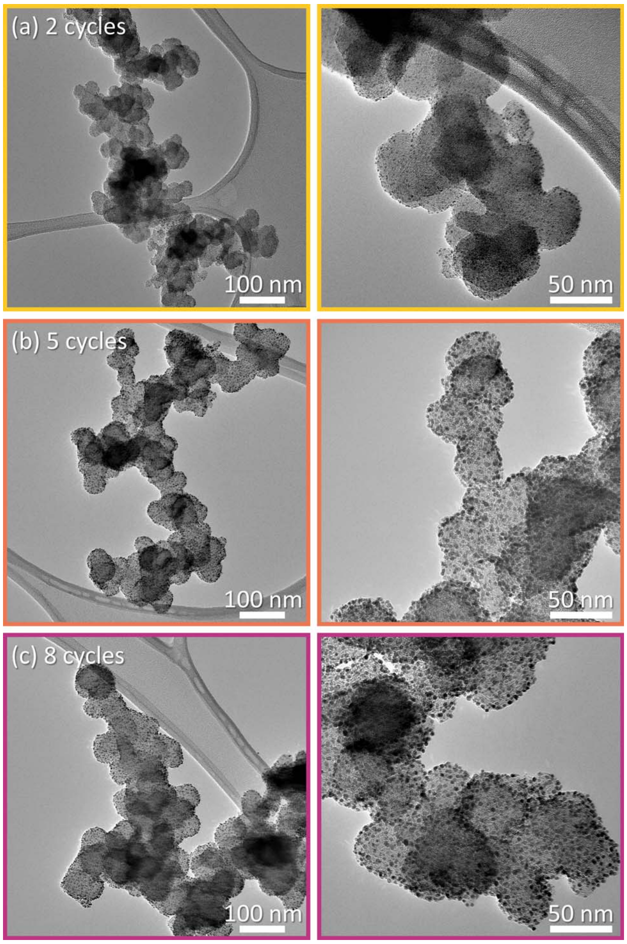

Fig. 7 Bright-field TEM micrographs of (a) ALD-Pt15/C, (b) ALD-Pt30/C, and (c) ALD-Pt40/C. All experiments have been conducted at the optimized oxygen dosage temperature of 150 °C.

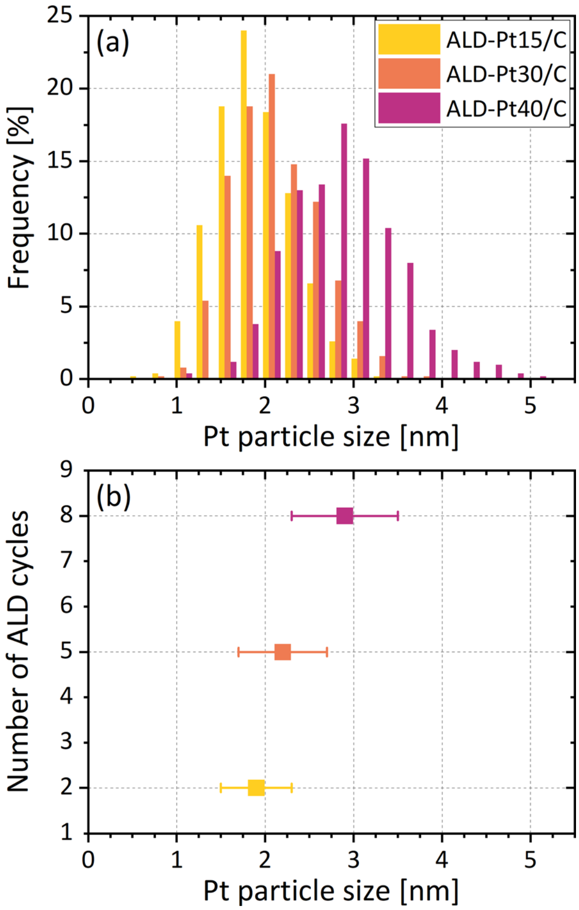

Fig. 8 (a) Pt particle size distributions of the different catalysts synthesized with different numbers of ALD cycles. The histograms were obtained by the evaluation of the corresponding 2D TEM micrographs. (b) Mean Pt nanoparticle diameter in relation to the number of ALD cycles applied.

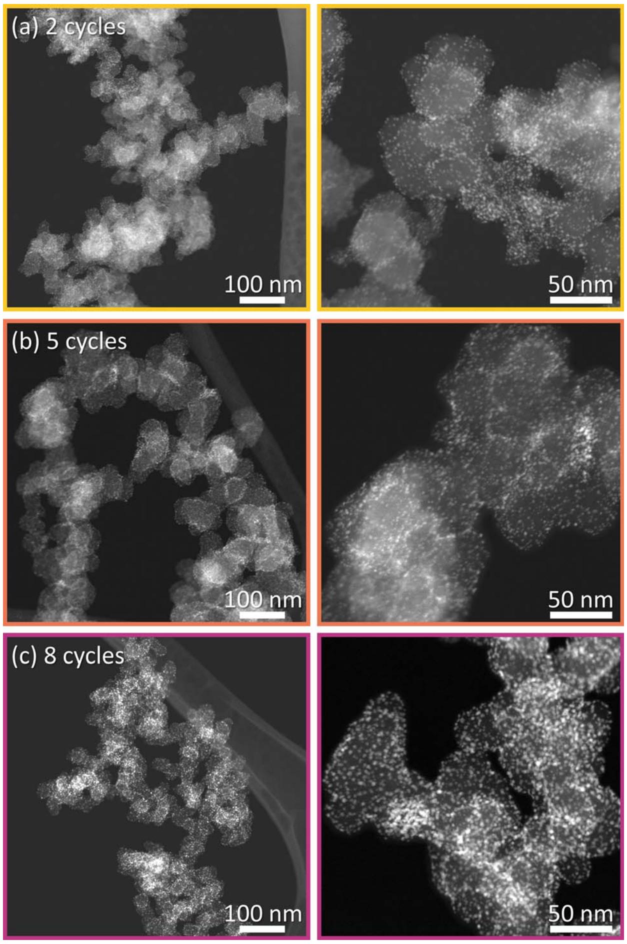

Fig. 9 Dark-field TEM micrographs of (a) ALD-Pt15/C, (b) ALD-Pt30/C, and (c) ALD-Pt40/C. All experiments have been conducted at the optimized oxygen dosage temperature of 150 °C.

increasing cycle count.[15] Overall, only nanoparticles and no larger agglomerates were found, indicating a homogeneous deposition without corrosion of the carbon support material.

HR-TEM micrographs highlighting platinum lattice fringes are given in Fig. 10. All catalysts show a lattice distance 0.22 nm, which is corresponding to the (111) facet of platinum.[15,43,44]

To further quantify these results, X-ray diffractograms were acquired (Fig. 11). The reflexes at $2\theta = 24°$ (002) and $2\theta = 43°$ (100) originate from the carbon support.[16,49] As more platinum is added into the system, the relative intensity of these reflexes decreases. Additionally, the (100) reflex is superimposed by the platinum reflexes at $2\theta = 39.7°$ (111) and $2\theta = 46.2°$ (200). For the sample with the fewest platinum ALD cycles, the diffractogram displays very broad platinum reflexes, stemming from non-pronounced crystallites.[27] With an increasing number of cycles and corresponding platinum content, the reflexes increase in intensity and become less broad, suggesting larger crystallites. However, all diffraction patterns lack sharp reflexes, indicating the presence only nanoparticles and the absence of bulk platinum particles in the sample. The crystallite sizes were calculated from the reflex at $2\theta = 67°$ (220) using the Scherrer equation[27] and are presented in Table 2. The values correlate well with the particle sizes observed in the TEM micrographs.

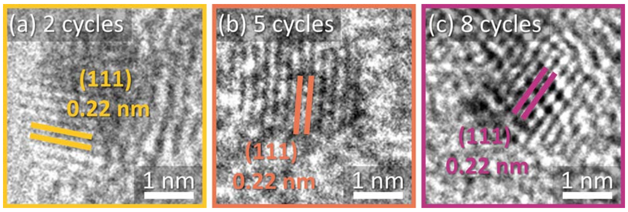

Fig. 10 HR-TEM micrographs of (a) ALD-Pt15/C, (b) ALD-Pt30/C, and (c) ALD-Pt40/C. All experiments have been conducted at the optimized oxygen dosage temperature of 150 °C.

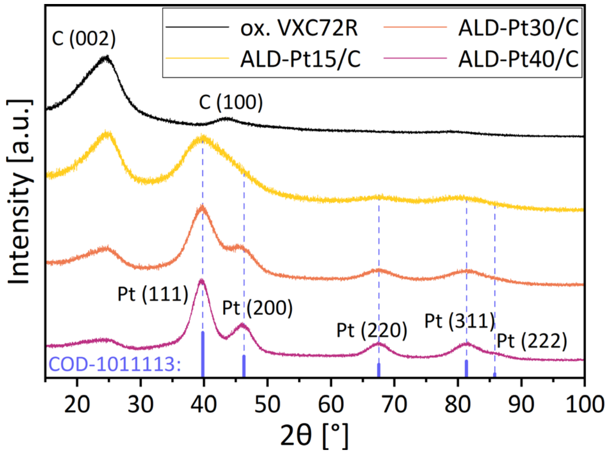

Fig. 11 Powder XRD pattern of the Pt/C catalysts prepared *via* ALD with varying platinum content as well as the oxidized carbon support.

In summary, by varying the ALD cycle number, the platinum content and particle size could be adjusted while maintaining highly dispersed platinum nanoparticles with a narrow size distribution. The two catalysts with higher platinum loading have been selected for further characterized in PEM fuel cell tests.

Electrochemical performance

The ALD catalysts with 30 wt% and 40 wt% platinum on carbon were benchmarked in an *in situ* fuel cell test and compared to a commercial Pt/C reference catalyst (TEC10V50E), which is also based on a similar Vulcan carbon support. BOT values for ECSA, mass activity, specific activity and Tafel slope are given in Table 3. Each electrocatalyst underwent 30 000 cycles of the U.S. DOE platinum dissolution test protocol, conducted between 0.6 V

Table 3 Electrochemical activity parameters measured of the characterized catalysts at BOT

Catalyst	ECSA [m^2 g$_{Pt}$$^{-1}$]	Mass activity [A g$_{Pt}$$^{-1}$]	Specific activity [mA cm$_{Pt}$$^{-2}$]	Tafel slope [mV dec^{-1}]
ALD-Pt30/C	55.1	84.0	0.153	82.3
ALD-Pt40/C	45.2	88.9	0.196	84.6
TEC10V50E	33.1	69.8	0.211	80.4

and 0.95 V, as outlined in the Experimental section. The electrochemical results are shown in Fig. 12(a).

The ALD-derived catalysts and the commercial Pt/C demonstrate comparable initial fuel cell performance in the activation, ohmic, and mass transport regions. After 30 000 AST cycles, a clear difference in performance decay can be observed between the reference catalyst and the ALD catalysts: at a voltage of 0.65 V, the cell with reference catalyst retains only 38% of its initial current density (Fig. 12(b)), whereas the ALD

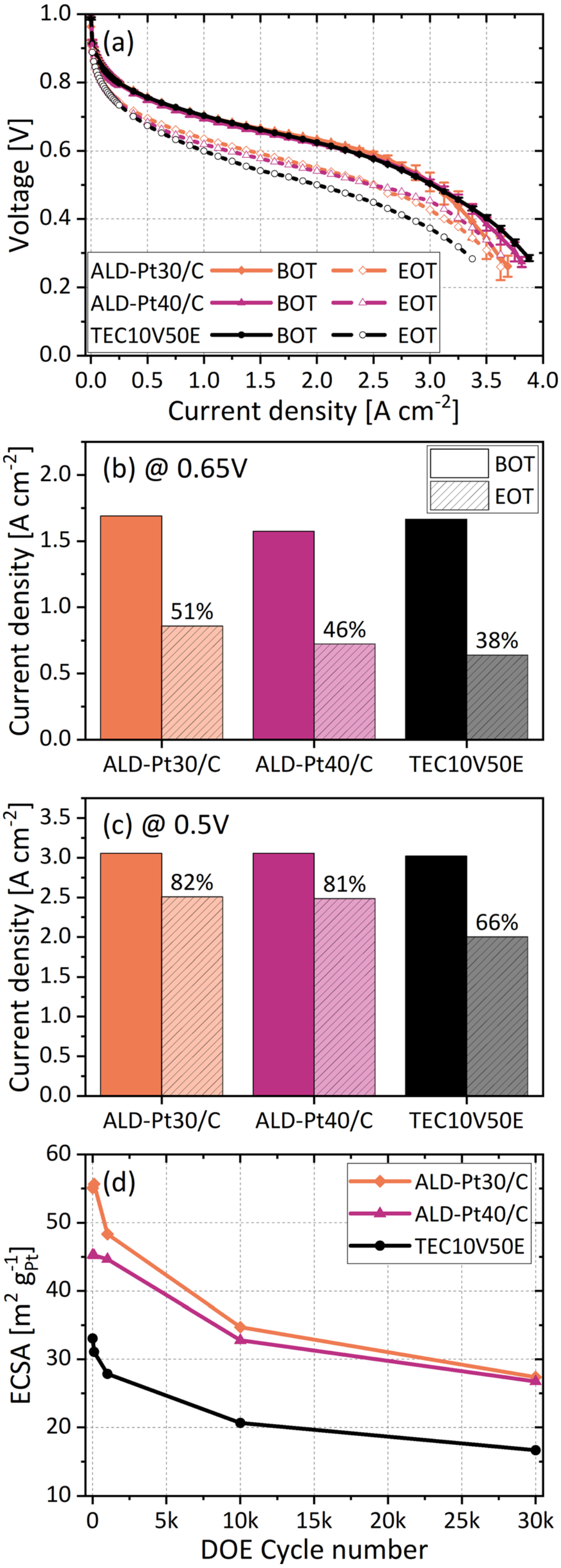

Fig. 12 Electrochemical characterization of the three electrocatalysts: (a) polarization curves in H_2/air at 80 °C, 50% RH and 130 kPa back pressure, (b) current densities taken at 0.65 V, (c) current densities taken at 0.5 V, and (d) ECSA determined from cyclic voltammograms measured in H_2/N_2, 80 °C, 100% RH and ambient pressure.

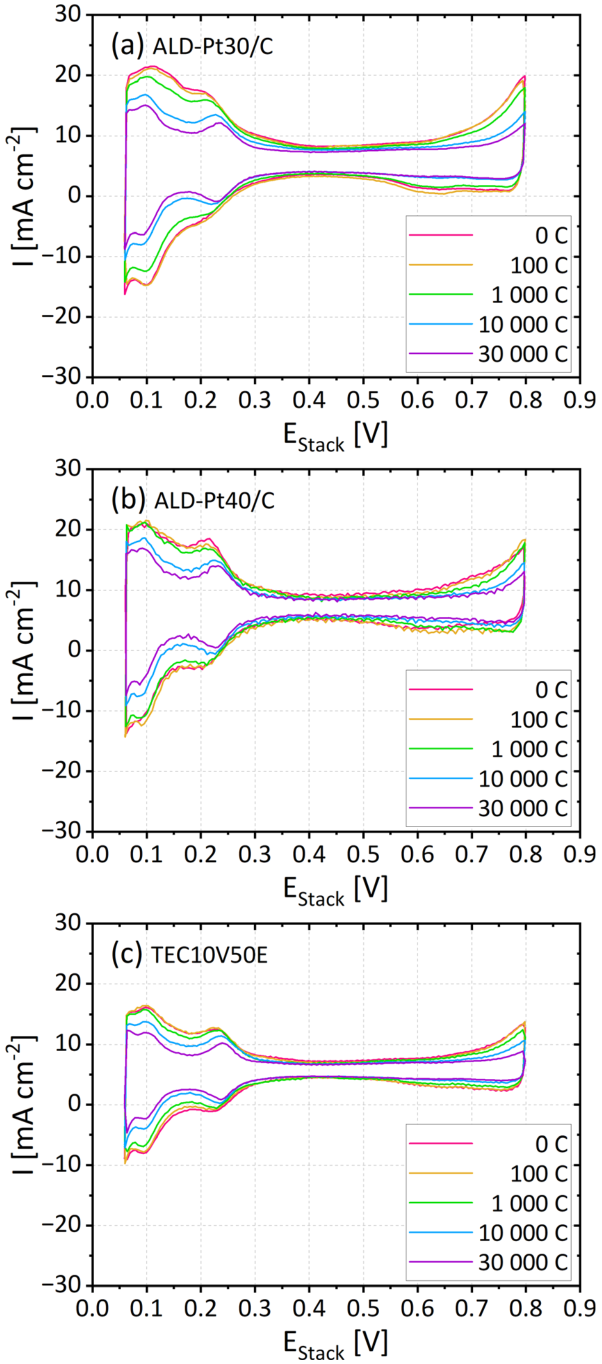

Fig. 13 CVs measured for (a) ALD-Pt30/C, (b) ALD-Pt40/C, and (c) TEC10V50E at BOT, after 100, 1000, 10 000 and 30 000 cycles.

catalysts retain a higher fraction of the initial current density (ALD-Pt30/C: 51% and ALD-Pt40/C: 46%). At a cell voltage of 0.5 V (Fig. 12(c)), this beneficial effect becomes even more obvious: both cells with ALD catalysts retain over 80% of their current density, whereas the commercial reference retains about 66% compared to BOT.

The ECSA was determined for each catalyst using cyclic voltammetry. The CVs taken at BOT and during accelerated degradation testing are given in Fig. 13. Fig. 12(d) shows the development of ECSA *versus* the number of AST cycles. At the beginning of cell testing, the ALD-Pt30/C catalyst exhibits a higher ECSA compared to the catalyst with 40 wt% platinum (Table 3). This can be attributed to its slightly smaller average platinum nanoparticle size, which was described in the previous section. As the cells undergo platinum degradation cycles, the platinum aggregates into larger particle sizes, causing the ECSAs of both materials to decrease. TEM micrographs of the EOT ALD catalysts are presented in Fig. 14. The anticipated and observed increase in platinum size is likely due to Ostwald ripening and agglomeration.[5,8] The dispersion of the nanoparticles on the carbon surface appears to be less homogeneous, which could further be explained by platinum detachment and dissolution.[5] The average platinum particle size determined from TEM increased from 2.2 ± 0.5 nm to 5.2 ± 1.5 nm for ALD-Pt30/C and from 2.9 ± 0.6 nm to 5.9 ± 1.5 nm for ALD-Pt40/C. These values fall within each other's margin of error, potentially explaining the similar ECSA values obtained for both catalysts between 1000 to 30 000 AST cycles.

Throughout the entire testing period, the ALD-prepared catalysts consistently exhibit 40 to 80% higher ECSAs and 20 to 50% higher mass activities in comparison to the commercial reference. For TEC10V50E, greater average platinum particle diameters and a broader particle size distributions,[50,51] with BOT platinum particle agglomerate sizes up to 10 nm,[52] have been reported, which could limit the electrochemically available surface area. The commercial catalyst can somewhat compensate for this by providing the highest specific activities (Table 3), however, for industrial application the mass activity is the more important metric, as it is directly related to the quantity of platinum needed and therefore PEM fuel cell cost.[53] Furthermore, the significantly less homogenous distribution of platinum on the carbon support[52–54] accelerates the degradation of platinum nanoparticles during AST through agglomeration and Ostwald ripening.[55] Conversely, the superior EOT performance and ECSA retention of the ALD catalysts can be attributed to the enhanced dispersion of the supported platinum nanoparticles across the carbon surface, coupled with a narrower platinum particle size distribution, increasing the stability of the catalyst against Ostwald ripening.[55]

These findings highlight the superior quality of the ALD-deposited catalyst material: Firstly, they exhibit highly dispersed platinum particles without the presence of agglomerates, resulting in superior ECSA. Secondly, due to their narrow size distribution, these materials are more stable against Ostwald ripening.[55] Even after 30 000 AST cycles, a higher degree of platinum particle surface remains electrochemically available, ensuring greater cell performance retention.

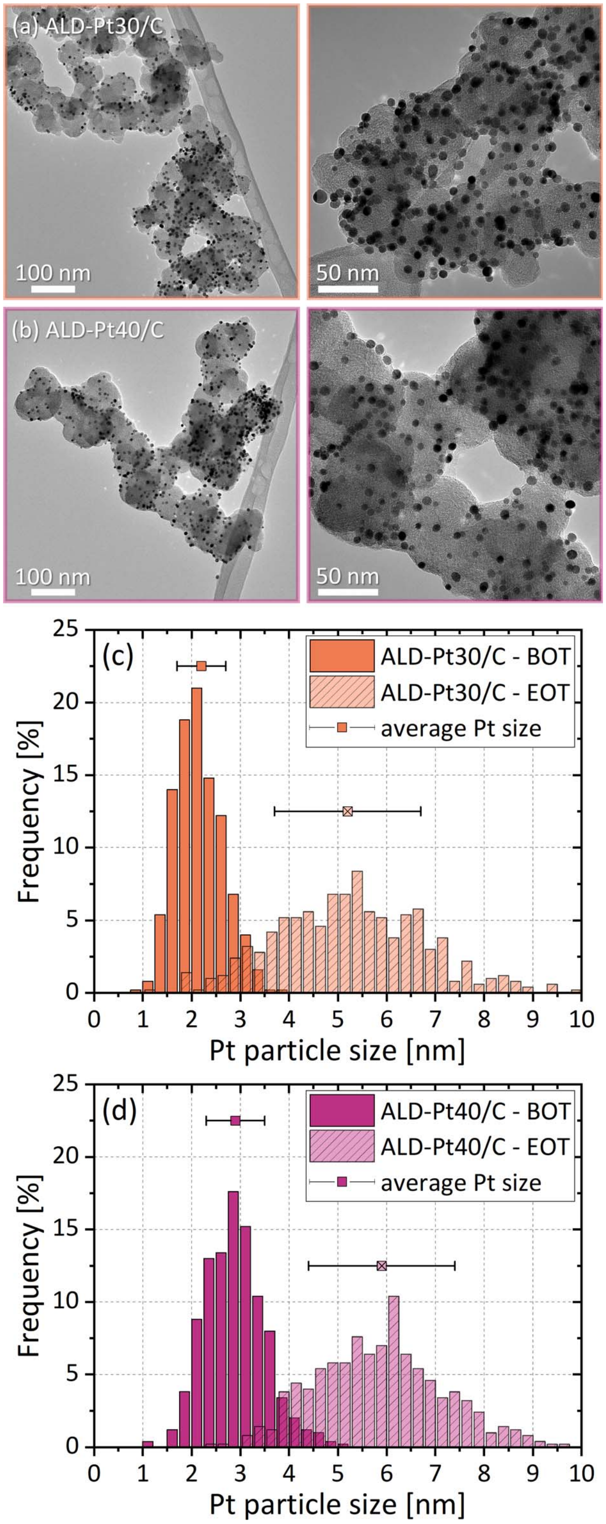

Fig. 14 TEM micrographs ((a) ALD-Pt30/C EOT, (b) ALD-Pt40/C EOT) and corresponding histograms (c) and (d) of ALD-derived catalysts before and after 30 000 cycles of AST.

Conclusions

In this study, we demonstrate the application of a commercial and scalable particle ALD system for synthesizing Pt/C catalysts for hydrogen fuel cells. By optimization of cycle temperatures and adjustment of the number of ALD cycles, we demonstrate the ability to fine-tune the platinum content on the carbon support while maintaining highly dispersed platinum nanoparticles characterized by a narrow size distribution (2.2 ± 0.5 nm for 30 wt% Pt/C). *In situ* fuel cell performance evaluation, in comparison to a commercial reference material, confirm their comparable performance, meeting typical metrics of current fuel cell performances (~1.6 A cm^{-2} at 0.65 V cell voltage). Furthermore, an accelerated stress test for platinum dissolution revealed significantly improved ECSA and cell performance retention for the ALD-derived catalysts. This enhancement can be attributed to the optimized platinum particle size distribution and homogeneous dispersion of platinum nanoparticles on the carbon support, achievable through the particle ALD process.

Future investigations will focus on extending this approach to deposit platinum onto alternative carbon support materials, with the aim of addressing the durability requirements outlined by current heavy-duty fuel cell development. Lastly, as the utilized commercial particle ALD system allows for the first time a scaled catalyst fabrication *via* ALD, we plan to conduct scale-up experiments, including the verification of the catalyst homogeneity, thereby paving the way for catalyst fabrication *via* ALD technology at a larger scale.

Data availability

The data supporting the findings of this study are included within the article.

Conflicts of interest

There are no conflicts to declare.

Acknowledgements

The authors acknowledge funding from the Federal Ministry of Education and Research of Germany (BMBF) through the projects Coral-HD (Grant 03SF0614A) and FC-RAT (Grant 03EW0011B). We would like to thank Miriam von Holst and Prof. Anna Fischer for insightful discussions regarding ALD, catalyst synthesis, and fuel cell characterization. Additionally, we thank Arberi Salihi for her experimental support in MEA fabrication and Miriam von Holst for her assistance with carbon oxidization experiments. The authors would also like to express their appreciation to Dr Yi Thomann and Dr Ralf Thomann for valuable discussions concerning TEM imaging and again to Dr Ralf Thomann for acquiring dark-field and HR-TEM micrographs and for performing d-spacing calculations. We thank Andreas Warmbold and Florian Mieβmer for conducting TGA measurements. Finally, we acknowledge Niklas Maier for his support with laboratory infrastructure planning and setup.

References

1 S. Pardhi, S. Chakraborty, D.-D. Tran, M. El Baghdadi, S. Wilkins and O. Hegazy, A Review of Fuel Cell Powertrains for Long-Haul Heavy-Duty Vehicles: Technology, Hydrogen, Energy and Thermal Management Solutions, *Energies*, 2022, **15**, 9557.

2 D. A. Cullen, K. C. Neyerlin, R. K. Ahluwalia, R. Mukundan, K. L. More, R. L. Borup, A. Z. Weber, D. J. Myers and A. Kusoglu, New roads and challenges for fuel cells in heavy-duty transportation, *Nat. Energy*, 2021, **6**, 462–474.

3 M. K. Debe, Electrocatalyst approaches and challenges for automotive fuel cells, *Nature*, 2012, **486**, 43–51.

4 M. Shao, Q. Chang, J.-P. Dodelet and R. Chenitz, Recent Advances in Electrocatalysts for Oxygen Reduction Reaction, *Chem. Rev.*, 2016, **116**, 3594–3657.

5 J. Zhao, H. Liu and X. Li, Structure, Property, and Performance of Catalyst Layers in Proton Exchange Membrane Fuel Cells, *Electrochem. Energy Rev.*, 2023, **6**, 13.

6 Z. Qiao, C. Wang, Y. Zeng, J. S. Spendelow and G. Wu, Advanced Nanocarbons for Enhanced Performance and Durability of Platinum Catalysts in Proton Exchange Membrane Fuel Cells, *Small*, 2021, **17**, e2006805.

7 J. C. Meier, C. Galeano, I. Katsounaros, J. Witte, H. J. Bongard, A. A. Topalov, C. Baldizzone, S. Mezzavilla, F. Schüth and K. J. J. Mayrhofer, Design criteria for stable Pt/C fuel cell catalysts, *Beilstein J. Nanotechnol.*, 2014, **5**, 44–67.

8 J. Wu, X. Z. Yuan, J. J. Martin, H. Wang, J. Zhang, J. Shen, S. Wu and W. Merida, A review of PEM fuel cell durability: Degradation mechanisms and mitigation strategies, *J. Power Sources*, 2008, **184**, 104–119.

9 S. Ding, H.-A. Chen, O. Mekasuwandumrong, M. J. Hülsey, X. Fu, Q. He, J. Panpranot, C.-M. Yang and N. Yan, High-temperature flame spray pyrolysis induced stabilization of Pt single-atom catalysts, *Appl. Catal., B*, 2021, **281**, 119471.

10 S. Ding, Y. Guo, M. J. Hülsey, B. Zhang, H. Asakura, L. Liu, Y. Han, M. Gao, J. Hasegawa, B. Qiao, T. Zhang and N. Yan, Electrostatic Stabilization of Single-Atom Catalysts by Ionic Liquids, *Chem*, 2019, **5**, 3207–3219.

11 J. Huang, Z. Chen, Q. He, W. Zhao, C. Zhu and Z. Chen, Inducing ionic interaction in Pt3CuN nanocatalysts for superior stability and CO-resilient towards methanol oxidation, *Mol. Catal.*, 2024, **564**, 114282.

12 Y. Lim, S. K. Kim, S.-C. Lee, J. Choi, K. S. Nahm, S. J. Yoo and P. Kim, One-step synthesis of carbon-supported Pd@Pt/C core-shell nanoparticles as oxygen reduction electrocatalysts and their enhanced activity and stability, *Nanoscale*, 2014, **6**, 4038–4042.

13 H. R. Colón-Mercado and B. N. Popov, Stability of platinum based alloy cathode catalysts in PEM fuel cells, *J. Power Sources*, 2006, **155**, 253–263.

14 H.-Y. Lee, T. H. Yu, C.-H. Shin, A. Fortunelli, S. G. Ji, Y. Kim, T.-H. Kang, B.-J. Lee, B. V. Merinov, W. A. Goddard, C. H. Choi and J.-S. Yu, Low temperature synthesis of new highly graphitized N-doped carbon for Pt fuel cell supports, satisfying DOE 2025 durability standards for both catalyst and support, *Appl. Catal., B*, 2023, **323**, 122179.

15 W.-J. Lee, S. Bera, H.-C. Shin, W.-P. Hong, S.-J. Oh, Z. Wan and S.-H. Kwon, Uniform and Size-Controlled Synthesis of Pt Nanoparticle Catalyst by Fluidized Bed Reactor Atomic

Layer Deposition for PEMFCs, *Adv. Mater. Interfaces*, 2019, **6**, 1901210.

16 W.-J. Lee, S. Bera, C. M. Kim, E.-K. Koh, W.-P. Hong, S.-J. Oh, E. Cho and S.-H. Kwon, Synthesis of highly dispersed Pt nanoparticles into carbon supports by fluidized bed reactor atomic layer deposition to boost PEMFC performance, *NPG Asia Mater.*, 2020, **12**, 1–13.

17 B. J. O'Neill, D. H. K. Jackson, J. Lee, C. Canlas, P. C. Stair, C. L. Marshall, J. W. Elam, T. F. Kuech, J. A. Dumesic and G. W. Huber, Catalyst Design with Atomic Layer Deposition, *ACS Catal.*, 2015, **5**, 1804–1825.

18 H. van Bui, F. Grillo and J. R. van Ommen, Atomic and molecular layer deposition: off the beaten track, *Chem. Commun.*, 2016, **53**, 45–71.

19 D. Longrie, D. Deduytsche and C. Detavernier, Reactor concepts for atomic layer deposition on agitated particles: A review, *J. Vac. Sci. Technol., A*, 2014, **32**, 10802.

20 A. M. Lubers, W. W. McNeary, D. J. Ludlow, A. W. Drake, M. Faust, M. E. Maguire, M. U. Kodas, M. Seipenbusch and A. W. Weimer, Proton Exchange Membrane Fuel Cell Flooding Caused by Residual Functional Groups after Platinum Atomic Layer Deposition, *Electrochim. Acta*, 2017, **237**, 192–198.

21 Forge Nano, Press Release – Atomic Layer Deposition Enabled Battery Materials, Methods and Products IP Roll-up, **https://www.forgenano.com/press-release-atomic-layer-deposition-enabled-battery-materials-methods-products-ip-roll/**, accessed 3 June 2024.

22 Forge Nano, Argonne National Laboratory Installs Forge Nano's Prometheus ALD tool to enable next gen ALD research and innovation, **https://www.forgenano.com/argonne-national-laboratory-installs-forge-nanos-prometheus-ald-tool-to-enable-next-gen-ald-research-and-innovation/**, accessed 3 June 2024.

23 Z. Zhao, G. Huang, Y. Kong, J. Cui, A. A. Solovev, X. Li and Y. Mei, Atomic Layer Deposition for Electrochemical Energy: from Design to Industrialization, *Electrochem. Energy Rev.*, 2022, **5**(Suppl 1), 31.

24 W.-J. Lee and S.-H. Kwon, Role of Acid Treatment of the Carbon Support in the Growth of Atomic-Layer-Deposited Pt Nanoparticles for PEMFC Fabrication, *Part. Part. Syst. Charact.*, 2022, 2200158.

25 Forge Nano, Announcing the Prometheus Series for Innovative ALD, **https://www.forgenano.com/announcing-prometheus-series-innovative-ald/**, accessed 3 June 2024.

26 Forge Nano, *PROMETHEUS*, **https://www.forgenano.com/wp-content/uploads/2022/12/ForgeNano_Equipment-Brochure_PROMETHEUS.pdf**, accessed 3 June 2024.

27 P. Scherrer, Bestimmung der Größe und der inneren Struktur von Kolloidteilchen mittels Röntgenstrahlen, *Nachr. Ges. Wiss. Goettingen, Math.-Phys. Kl.*, 1918, **1918**, 98–100.

28 J. I. Langford and A. J. C. Wilson, Scherrer after sixty years: A survey and some new results in the determination of crystallite size, *J. Appl. Crystallogr.*, 1978, **11**, 102–113.

29 I. N. Leontyev, A. B. Kuriganova, M. Allix, A. Rakhmatullin, P. E. Timoshenko, O. A. Maslova, A. S. Mikheykin and N. V. Smirnova, On the Evaluation of the Average Crystalline Size and Surface Area of Platinum Catalyst Nanoparticles, *Phys. Status Solidi B*, 2018, **255**, 1800240.

30 H. Nguyen, F. Lombeck, C. Schwarz, P. A. Heizmann, M. Adamski, H.-F. Lee, B. Britton, S. Holdcroft, S. Vierrath and M. Breitwieser, Hydrocarbon-based Pemion™ proton exchange membrane fuel cells with state-of-the-art performance, *Sustainable Energy Fuels*, 2021, **5**, 3687–3699.

31 K. Yildirim, H. Fadlullah, C. Schwarz, F. Lombeck, C. Klose, S. Vierrath and M. Breitwieser, 30 μm Thin Anode Gas Diffusion Layers for Optimized PEM Fuel Cell Operation at 120 °C and Low Relative Humidity, *Adv. Energy Sustainability Res.*, 2024, **5**, 2300179.

32 P. A. Heizmann, H. Nguyen, M. von Holst, A. Fischbach, M. Kostelec, F. J. Gonzalez Lopez, M. Bele, L. Pavko, T. Đukić, M. Šala, F. Ruiz-Zepeda, C. Klose, M. Gatalo, N. Hodnik, S. Vierrath and M. Breitwieser, Alternative and facile production pathway towards obtaining high surface area PtCo/C intermetallic catalysts for improved PEM fuel cell performance, *RSC Adv.*, 2023, **13**, 4601–4611.

33 J. Stiegeler, T. Mittermeier, L. Tsikonis, T. Lehre and S. Vierrath, Influence Factors of Platinum Dissolution in Proton Exchange Membrane Fuel Cells: A Sensitivity Study, *J. Electrochem. Soc.*, 2024, **171**, 054517.

34 U.S. Department of Energy (DOE) Fuel Cell Technologies Office (FCTO), *Fuel Cells Multi-Year Research Development and Demonstration Plan*, 2016, accessed 18 March 2024.

35 H. Schulenburg, J. Durst, E. Müller, A. Wokaun and G. G. Scherer, Real surface area measurements of Pt3Co/C catalysts, *J. Electroanal. Chem.*, 2010, **642**, 52–60.

36 H. Liepold, H. Nguyen, P. A. Heizmann, C. Klose, S. Vierrath and A. Münchinger, Gas Transport Resistance of Hydrocarbon-Based Catalyst Layers in Proton-Exchange Membrane Fuel Cells, *J. Electrochem. Soc.*, 2024, **171**, 54509.

37 H. Nguyen, D. Sultanova, P. A. Heizmann, S. Vierrath and M. Breitwieser, Improving the efficiency of fully hydrocarbon-based proton-exchange membrane fuel cells by ionomer content gradients in cathode catalyst layers, *Mater. Adv.*, 2022, **3**, 8460–8468.

38 U.S. Department of Energy (DOE), *FuelCell Technical Team Roadmap*, 2017, accessed 16 August 2024.

39 K. C. Neyerlin, W. Gu, J. Jorne and H. A. Gasteiger, Determination of Catalyst Unique Parameters for the Oxygen Reduction Reaction in a PEMFC, *J. Electrochem. Soc.*, 2006, **153**, A1955.

40 T. Aaltonen, M. Ritala, T. Sajavaara, J. Keinonen and M. Leskelä, Atomic Layer Deposition of Platinum Thin Films, *Chem. Mater.*, 2003, **15**, 1924–1928.

41 A. M. Lubers, C. L. Muhich, K. M. Anderson and A. W. Weimer, Mechanistic studies for depositing highly dispersed Pt nanoparticles on carbon by use of trimethyl(methylcyclopentadienyl)platinum(IV) reactions with O2 and H2, *J. Nanopart. Res.*, 2015, **17**, 1–16.

42 C. Gump, A. A. Dameron, B. Boeyink and S. Harris, Scale Up of ALD of Platinum Onto Carbon Powder in Fluidized Beds for Fuel Cell Applications, *Meet. Abstr.*, 2021, **MA2021-02**, 891.

43 S. Sui, X. Wang, X. Zhou, Y. Su, S. Riffat and C. Liu, A comprehensive review of Pt electrocatalysts for the oxygen reduction reaction: Nanostructure, activity, mechanism and carbon support in PEM fuel cells, *J. Mater. Chem. A*, 2017, **5**, 1808–1825.

44 M. Shakoorioskooie, Y. Z. Menceloglu, S. Unal and S. Hayat Soytas, Rapid Microwave-Assisted Synthesis of Platinum Nanoparticles Immobilized in Electrospun Carbon Nanofibers for Electrochemical Catalysis, *ACS Appl. Nano Mater.*, 2018, **1**, 6236–6246.

45 W. P. Davey, Precision Measurements of the Lattice Constants of Twelve Common Metals, *Phys. Rev.*, 1925, **25**, 753–761.

46 S. Gražulis, D. Chateigner, R. T. Downs, A. F. T. Yokochi, M. Quirós, L. Lutterotti, E. Manakova, J. Butkus, P. Moeck and A. Le Bail, Crystallography Open Database - an open-access collection of crystal structures, *J. Appl. Crystallogr.*, 2009, **42**, 726–729.

47 S. Gražulis, A. Daškevič, A. Merkys, D. Chateigner, L. Lutterotti, M. Quirós, N. R. Serebryanaya, P. Moeck, R. T. Downs and A. Le Bail, Crystallography Open Database (COD): an open-access collection of crystal structures and platform for world-wide collaboration, *Nucleic Acids Res.*, 2012, **40**, D420–D427.

48 V. S. Pinheiro, F. M. Souza, T. C. Gentil, P. Böhnstedt, E. C. Paz, L. S. Parreira, P. Hammer, B. L. Batista and M. C. Santos, Insights in the Study of the Oxygen Reduction Reaction in Direct Ethanol Fuel Cells using Hybrid Platinum-Ceria Nanorods Electrocatalysts, *ChemElectroChem*, 2019, **6**, 5124–5135.

49 N. S. Saenko, The X-ray diffraction study of three-dimensional disordered network of nanographites: Experiment and theory, *Phys. Procedia*, 2012, **23**, 102–105.

50 G. S. Harzer, J. N. Schwämmlein, A. M. Damjanović, S. Ghosh and H. A. Gasteiger, Cathode Loading Impact on Voltage Cycling Induced PEMFC Degradation: A Voltage Loss Analysis, *J. Electrochem. Soc.*, 2018, **165**, F3118–F3131.

51 E. Remy, Y. Thomas, L. Guetaz, F. Fouda-Onana, P.-A. Jacques and M. Heitzmann, Optimization and Tunability of 2D Graphene and 1D Carbon Nanotube Electrocatalysts Structure for PEM Fuel Cells, *Catalysts*, 2018, **8**, 377.

52 T. Ito, U. Matsuwaki, Y. Otsuka, M. Hatta, K. Hayakawa, K. Matsutani, T. Tada and H. Jinnai, Three-Dimensional Spatial Distributions of Pt Catalyst Nanoparticles on Carbon Substrates in Polymer Electrolyte Fuel Cells, *Electrochemistry*, 2011, **79**, 374–376.

53 R. Riasse, C. Lafforgue, F. Vandenberghe, F. Micoud, A. Morin, M. Arenz, J. Durst and M. Chatenet, Benchmarking proton exchange membrane fuel cell cathode catalyst at high current density: A comparison between the rotating disk electrode, the gas diffusion electrode and differential cell, *J. Power Sources*, 2023, **556**, 232491.

54 R. Sgarbi, W. Ait Idir, Q. Labarde, M. Mermoux, P. Wu, J. Mainka, J. Dillet, C. Marty, F. Micoud, O. Lottin and M. Chatenet, Does the platinum-loading in proton-exchange membrane fuel cell cathodes influence the durability of the membrane-electrode assembly?, *Ind. Chem. Mater.*, 2023, **1**, 501–515.

55 S. Hu and W.-X. Li, Influence of Particle Size Distribution on Lifetime and Thermal Stability of Ostwald Ripening of Supported Particles, *ChemCatChem*, 2018, **10**, 2900–2907.